

GA-A27316

EFFECT OF SEPARATRIX MAGNETIC GEOMETRY ON DIVERTOR BEHAVIOR IN DIII-D

by

**T.W. PETRIE, J.M. CANIK, C.J. LASNIER, A.W. LEONARD, M.A. MAHDAVI,
J.G. WATKINS, M.E. FENSTERMACHER, J.R. FERRON, R.J. GROEBNER, D.N. HILL,
A.W. HYATT, C.T. HOLCOMB, T.C. LUCE, R.A. MOYER, and P.C. STANGEBY**

MAY 2012



DISCLAIMER

This report was prepared as an account of work sponsored by an agency of the United States Government. Neither the United States Government nor any agency thereof, nor any of their employees, makes any warranty, express or implied, or assumes any legal liability or responsibility for the accuracy, completeness, or usefulness of any information, apparatus, product, or process disclosed, or represents that its use would not infringe privately owned rights. Reference herein to any specific commercial product, process, or service by trade name, trademark, manufacturer, or otherwise, does not necessarily constitute or imply its endorsement, recommendation, or favoring by the United States Government or any agency thereof. The views and opinions of authors expressed herein do not necessarily state or reflect those of the United States Government or any agency thereof.

GA-A27316

EFFECT OF SEPARATRIX MAGNETIC GEOMETRY ON DIVERTOR BEHAVIOR IN DIII-D

by

T.W. PETRIE, J.M. CANIK,* C.J. LASNIER,[†] A.W. LEONARD, M.A. MAHDAVI,
J.G. WATKINS,[‡] M.E. FENSTERMACHER,[†] J.R. FERRON, R.J. GROEBNER, D.N. HILL,[†]
A.W. HYATT, C.T. HOLCOMB,[†] T.C. LUCE, R.A. MOYER[¶], and P.C. STANGEBY[§]

This is a preprint of a paper to be presented at the Twentieth International Conference on Plasma-Surface Interactions in Controlled Fusion Devices, May 21–25, 2012 in Aachen, Germany and to be published in the *J. Nucl. Mater.*

*Oak Ridge National Laboratory, Oak Ridge, Tennessee, USA.

[†]Sandia National Laboratories, Albuquerque, New Mexico, USA.

[‡]Lawrence Livermore National Laboratory, Livermore, California, USA.

[¶]University of California San Diego, La Jolla, California, USA.

[§]University of California San Diego, La Jolla, California, USA.

**Work supported in part by
the U.S. Department of Energy under
DE-FC02-04ER54698, DE-AC05-00OR22725, DE-AC52-07NA28344,
DE-AC04-94AL85000, and DE-FG02-07ER54917**

**GENERAL ATOMICS PROJECT 30200
MAY 2012**



Paper O-36**Effect of separatrix magnetic geometry on divertor behavior in DIII-D**

**T.W. Petrie^{a*}, J.M. Canik^b, C.J. Lasnier^c, A.W. Leonard^a, M.A. Mahdavi^a,
J.G. Watkins^d, M.E. Fenstermacher^c, J.R. Ferron^a, R.J. Groebner^a, D.N. Hill^c,
A.W. Hyatt^a, C.T. Holcomb^c, T.C. Luce^a, R.A. Moyer^e, and P.C. Stangeby^f**

^a*General Atomics, P.O. Box 85608, San Diego, California 92186-5608, USA.*

^b*Oak Ridge National Laboratory, P.O. Box 2008, Oak Ridge, Tennessee 37831, USA.*

^c*Lawrence Livermore National Laboratory, Livermore, California 94550, USA.*

^d*Sandia National Laboratories, P.O. Box 5800, Albuquerque, New Mexico 87185, USA.*

^e*University of California-San Diego, La Jolla, California 92093-0417, USA.*

^f*University of Toronto Institute of Aerospace Studies, Toronto, Canada*

Abstract We report on recent experiments on DIII-D that examined the effects that variations in the parallel connection length in the scrape-off layer (SOL), L_{\parallel} , and the radial location of the outer divertor target, R_{TAR} , have on divertor plasma properties. Two-point modeling of the SOL plasma predicts that larger values of L_{\parallel} and R_{TAR} should lower temperature and raise density at the outer divertor target for fixed upstream separatrix density and temperature, i.e., $n_{\text{TAR}} \propto [R_{\text{TAR}}]^2 [L_{\parallel}]^{4/7}$ and $T_{\text{TAR}} \propto [R_{\text{TAR}}]^{-2} [L_{\parallel}]^{-6/7}$. The dependence of n_{TAR} and T_{TAR} on L_{\parallel} was consistent with our data, but the dependence of n_{TAR} and T_{TAR} on R_{TAR} was not. The surprising result that the divertor plasma parameters did not depend on R_{TAR} in the predicted way may be due to convected heat flux, driven by escaping neutrals, in the more open configuration of the larger R_{TAR} cases. Modeling results using the SOLPS code support this postulate.

PACS: 52.25Ya, 52.55.Fa, 52.55.Rk, 89.30.Jj

1. INTRODUCTION

Future highly powered tokamaks will require some means of reducing damaging steady and transient (ELM-induced) power loading at the divertor targets. Previous investigations have demonstrated that the steady heat loads can be significantly reduced by approaches involving the radiating divertor concept [1–4], although scaling this approach to future generation tokamaks is still at present problematical.

Other approaches exploit divertor geometry to dissipate high levels of power loading at the divertor target, e.g., the Super-X [5] and Snowflake [6] concepts. In theory, power flow into the divertor can be dissipated and divertor temperature lowered by increasing the distance that heat from the main plasma entering the scrape-off layer (SOL) must traverse along a magnetic field line to the divertor target or by raising the radial isolation of the outer divertor target. These ideas are based on well-understood physics in the SOL and can best be expressed at its simplest level by this formulation of the one-dimensional Two-Point Model (TPM) [7]:

$$T_{\text{TAR}} \propto [P_{\text{IN}}(1 - f_{\text{RAD}})]^{10/7} (R_{\text{TAR}} n_{\text{SEP}})^{-2} \left\{ (f_R - 1) / [L_{\parallel} \ln(f_R)] \right\}^{4/7}, \quad (1)$$

and

$$n_{\text{TAR}} \propto [R_{\text{TAR}}]^2 [n_{\text{TAR}}]^3 [P_{\text{IN}}(1 - f_{\text{RAD}})]^{-8/7} \left\{ [L_{\parallel} \ln(f_R)] / (f_R - 1) \right\}^{6/7}, \quad (2)$$

where R_{TAR} is the radial location of the outer divertor separatrix target, L_{\parallel} is a representative parallel connection length in the SOL between the midplane (or X-point) and the divertor target, n_{TAR} is the electron density at the outer divertor target, T_{TAR} is the electron temperature at the outer divertor target, n_{SEP} is the upstream electron density on the separatrix, P_{IN} is the power input, f_{RAD} is the fraction of radiated power, and f_R is the ratio $R_{\text{TAR}}/R_{\text{OMP}}$, where R_{OMP} is the radial location of the outer midplane. These simple scalings suggest that conditions conducive to a radiative divertor solution can be achieved at lower n_{SEP} by increasing either R_{TAR} or L_{\parallel} . We report results and interpretation of recent experiments on DIII-D designed to evaluate divertor geometries that might be favorable for radiative heat dispersal by testing how specific variations in R_{TAR} and L_{\parallel} affect n_{TAR} , T_{TAR} , and heat flux at the outer divertor target.

2. EXPERIMENT

Three of the main plasma shapes used in this study are shown in Fig. 1. The maximum variation in radial placement of the outer divertor separatrix R_{TAR} for these lower single-nulls (SN) ranged from 1.20 m (black) to 1.67 m (green), as shown in Fig. 1. In later discussion, we distinguish between two regions of the divertor: *floor* and *baffle top*, as shown. The minimum and maximum *poloidal* extensions from the X-point to the outer divertor target for the plasmas in this experiment were 0.25 m (red) to 0.75 m (black), respectively, in Fig. 1. These poloidal distances correspond to parallel connection lengths $L_{\parallel-\text{XPT}}$ of 17 m and 25 m, which constitute $\approx 50\%-55\%$ and $\approx 60\%-65\%$ of the parallel connection lengths between the outer divertor target and the outer midplane ($L_{\parallel-\text{MID}}$), respectively. By contrast, the *poloidal* distances from the X-point to the vertical *inner* divertor target for the cases studied were between 0.1–0.2 m, corresponding to parallel connection lengths of 6–8 m. In all cases, the parallel path lengths in the SOL are referenced to the flux surface 0.15 cm radially outside the outer midplane separatrix.

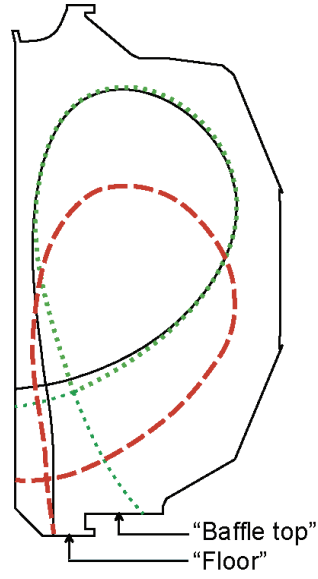


Fig. 1. The poloidal cross-sections of the MHD equilibria for three important cases discussed in this paper are shown. The floor and baffle top regions of the lower divertor are indicated.

Upstream electron density and temperature were determined by Thomson scattering, while electron density and temperature downstream at the *outer* divertor target were determined from Langmuir probe measurements. No Langmuir probe measurements were available at the *inner* divertor target. Heat flux across the divertor was determined from infrared camera measurements taken between ELMs.

This experiment included both H-mode and L-mode plasmas. The ion $\mathbf{B} \times \nabla B$ drift was directed *toward* the X-point in all cases. There was no active particle pumping. $Z_{\text{eff}} \approx 1.3\text{--}1.5$ and was mostly due to carbon. The outer divertor target was attached at all times, but the inner divertor target was detached (or, at most, weakly attached) between ELMs.

3. RESULTS

3.1. Preliminary assessment of the dependence of n_{TAR} and T_{TAR} on R_{TAR}

Two matched ELMing H-mode plasmas provided the data for comparison to Eqns (1) and (2), since their respective R_{TAR} represent the widest range possible in this experiment, i.e., 1.20 m (black) and 1.67 m (green) in Fig. 1. For either case, $n_e/n_G \approx 0.4$, $H_{89P} \approx 1.6$, and $P_{\text{RAD}}/P_{\text{IN}} \approx 0.4$. Edge and divertor properties are summarized in Table 1. The dependence of n_{TAR} and T_{TAR} did not follow TPM predictions of Eqns (1) and (2), i.e., n_{TAR} should *increase* by $\approx 20\%$ and T_{TAR} should *decrease* by $\approx 26\%$ between the $R_{\text{TAR}} = 1.20$ m and 1.67 m. From experiment, however, n_{TAR} decreased by $\approx 51\%$ and T_{TAR} increased by $\approx 33\%$, lower T_{SEP} (Table I). In addition, the peak heat flux $[Q_{\perp}]^{\text{IR}}$, based on infrared camera data, was $\approx 25\%$ higher for the $R_{\text{TAR}} = 1.67$ m case.

Table 1
Large R_{TAR} vs low R_{TAR}

	Low R_{TAR}	High R_{TAR}
$L_{\parallel-\text{XPT}}$ (m)	25 [40]	20 [32]
R_{TAR} (m)	1.20	1.67
$n_{\text{SEP}} \left(10^{19} \text{ m}^{-3}\right)$	0.91	0.92
T_{SEP} (eV)	91	71
$n_{\text{TAR}} \left(10^{19} \text{ m}^{-3}\right)$	3.4	1.7
T_{TAR} (eV)	18.0	24.0
$[Q_{\perp}]^{\text{IR}} \left(\text{MW/m}^2\right)$	1.2	1.5

3.2. Outer strike point sweep in L-mode

A radial sweep of the outer strike point (OSP) across both floor and baffle top is helpful in establishing what may be happening *between* these R_{TAR} endpoints. An L-mode plasma was used to avoid sizable variation in core plasma properties that would occur in ELMing H-mode plasmas over such large sweeps in R_{TAR} . The endpoints of this sweep in L-mode were $R_{\text{TAR}} = 1.20$ m and 1.60 m. Both n_{TAR} and T_{TAR}

qualitatively track the predictions of the TPM across the floor and across the baffle top, when considered *separately*, but have much stronger dependences on R_{TAR} along the *floor* than along the *baffle top*. Figure 2 also suggests a discontinuity in R_{TAR} across the floor-baffle top boundary for both n_{TAR} and T_{TAR} . Note that when considering the n_{TAR} and T_{TAR} values at the *endpoints* of the sweep, the results in Sec. 3.1 are qualitatively recovered.

3.3. Outer strike point sweep in H-mode

A slower radial sweep of the OSP limited only to the floor examined the effect of the proximity of the OSP to the baffle facing at $R = 1.37$ m. ELMing H-mode properties remained virtually constant over this sweep due to its limited range (i.e., $R_{\text{TAR}} = 1.21$ – 1.30 m). As in the L-mode case, the responses of n_{TAR} and T_{TAR} to changes in R_{TAR} were stronger than expected from TPM (Fig. 3). Since the sweep did not extend onto the baffle top, a second shot was added to Fig. 3 for comparison, which had similar edge plasma properties. No monotonic continuity in R_{TAR} for either n_{TAR} or T_{TAR} was apparent across the floor and baffle top boundary. $[Q_{\perp}]^{\text{IR}}$ was lowest when R_{TAR} was closer to the baffle structure on the floor, i.e., $R_{\text{TAR}} = 1.30$ m (Fig. 4).

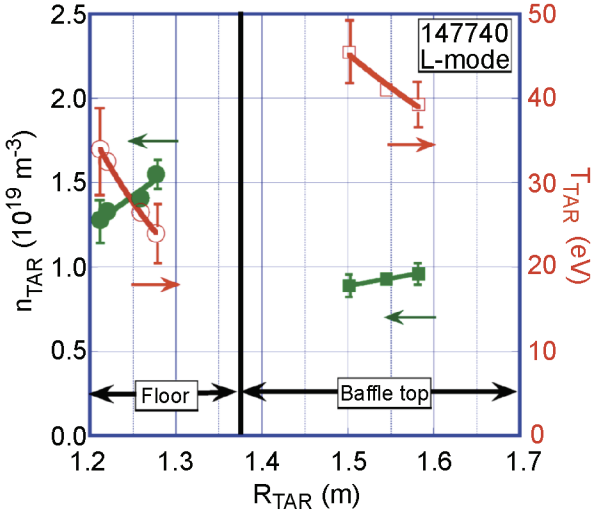


Fig. 2. n_{TAR} (closed) and T_{TAR} (open) at the OSP are shown as a function of R_{TAR} . This *L-mode* shot is characterized by: $I_p = 0.8$ MA, $q_{95} = 3.8$, $P_{\text{IN}} = 1.2$ MW, $H_{89\text{P}} \approx 1.0$, $P_{\text{RAD}}/P_{\text{IN}} \approx 0.35$ and $n_e/n_G \approx 0.2$.

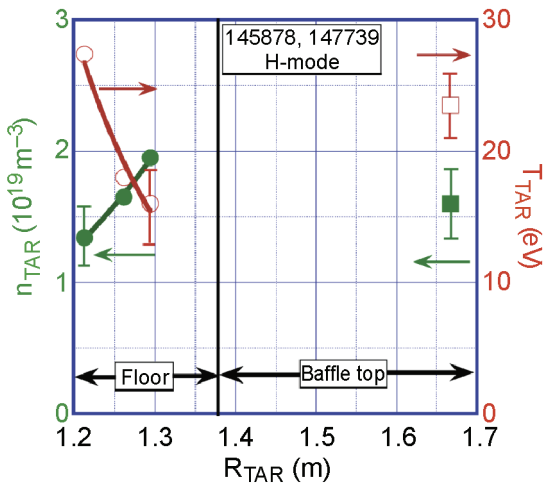


Fig. 3. n_{TAR} (closed) and T_{TAR} (open) at the OSP are shown as a function of R_{TAR} . This *H-mode* shot is characterized by: $I_p = 0.8$ MA, $q_{95} = 4.3$, $P_{\text{IN}} = 4.9$ MW, $H_{89\text{P}} \approx 1.9$, $P_{\text{RAD}}/P_{\text{IN}} \approx 0.35$ and $n_e/n_G \approx 0.3$.

3.4. Variation of n_{TAR} and T_{TAR} with L_{\parallel}

T_{TAR} Equations (1) and (2) predict that lengthening the outer divertor leg increases n_{TAR} and decreases T_{TAR} . To test this prediction, we compared two H-mode plasmas having significantly different L_{\parallel} but virtually the same R_{TAR} . Their shapes are shown as the black (high X-point) and red (low X-point) curves in Fig. 1. Table 2 shows that the case with larger L_{\parallel} (high X-point) resulted in higher n_{TAR} and lower T_{TAR} . More quantitatively, Eqns (1) and (2) can be combined with data from the low X-point case (Table 2) to extrapolate n_{TAR} and lower in the high X-point case. If we use $L_{\parallel-\text{XPT}}$ as the connection length, then the two-point model predicts the longer parallel connection length (higher X-point) case: $n_{\text{TAR}} \approx 4.6 \times 10^{19} \text{ m}^{-3}$ and $T_{\text{TAR}} \approx 17 \text{ eV}$. These are in quantitative agreement with the actual measurements (Table 2). Although the poloidal flux expansion at the outer divertor target (f_{EXP}) was ≈ 3.2 in the high X-point case and ≈ 5.6 in the low X-point case, $[Q_{\perp}]^{\text{IR}}$ was greater in the latter (Table 2). The FWHM was 3.5 cm in both cases.

Table 2
High X-point vs low X-point

	High X-point	Low X-point
$L_{\parallel-\text{XPT}}$ (m)	25	17
R_{TAR} (m)	1.20	1.21
$n_{\text{SEP}} \left(10^{19} \text{ m}^{-3}\right)$	1.03	1.01
T_{SEP} (eV)	74	84
$n_{\text{TAR}} \left(10^{19} \text{ m}^{-3}\right)$	4.4	3.2
T_{TAR} (eV)	17.0	21.5
$[Q_{\perp}]^{\text{IR}} \left(\text{MW/m}^2\right)$	1.0	1.15

4. DISCUSSION AND SUMMARY

Modeling of the edge and divertor plasmas was done using the SOLPS suite of codes [8], which provide a 2-D model to couple plasma and neutral transport. The plasma transport was calculated using the fluid code B2 [9] and the neutral transport was calculated using the Monte-Carlo code EIRENE [10]. Classical drifts were not included. SOLPS was used in an interpretive sense, with the primary constraint being the measured midplane density and temperature profiles, which were matched in the simulation using radially varying, poloidally constant transport coefficients [11]. No anomalous convection was included, so these represent “effective” cross-field diffusivities. The measured divertor heat flux effectively constrained the position of the midplane profiles relative to the separatrix. With the midplane data matched to the measured profiles, the simulated divertor density and temperature profiles were then compared to the measured values rather than constrained by them directly.

SOLPS calculations for the two R_{TAR} cases discussed in Sec. 3.1 show that n_{TAR} , T_{TAR} , and Q_{\perp} are in qualitative agreement with experiment, as shown in Fig. 5. SOLPS modeling indicates that n_{TAR} is higher and both T_{TAR} and Q_{\perp} are lower for the low $R_{\text{TAR}} = 1.20 m (black) case. Both T_{TAR} and Q_{\perp} are in good quantitative agreement with the data, although the experimental n_{TAR} is roughly a factor of two higher in either R_{TAR} case. (Divertor density calculated by SOLPS may be lower than the measured density because calculated ion temperature at the divertor target may be too high, requiring a lower density to match the measured heat flux.) More neutrals escape the outer divertor target in the more open configuration ($R_{\text{TAR}} = 1.67 m case). A fraction of these neutrals return upstream of the target, are ionized, and flow back to the target, thereby increasing the convective component of the power flow to the divertor target more than would occur in the more closed configuration ($R_{\text{TAR}} = 1.20 m case). Increasing the convective component of the power flow would increase T_{TAR} and reduce n_{TAR} [12]. For a location slightly upstream of the divertor target, SOLPS modeling shows that, for the $R_{\text{TAR}} = 1.67$ m case, convection carries virtually the entire heat flux outside the radial location of the FWHM of Q_{\perp} , while for the $R_{\text{TAR}} = 1.20$ m case at FWHM of Q_{\perp} , conduction still plays a substantial role (~30%).$$$

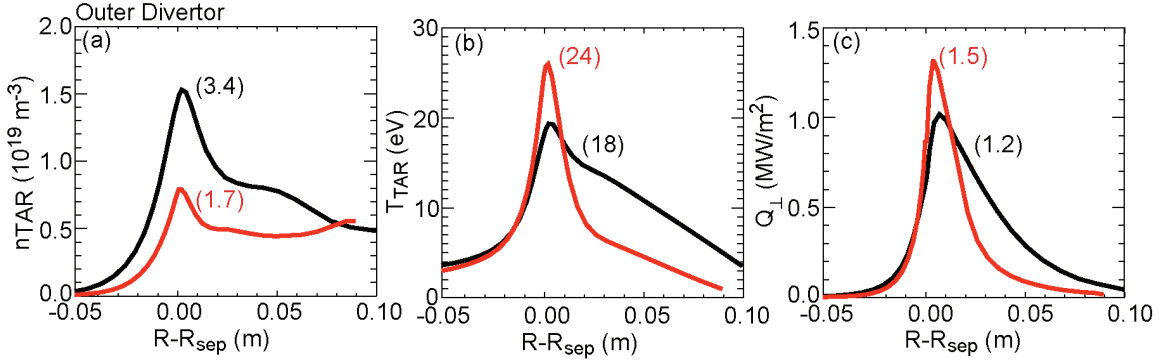


Fig. 5. SOLPS modeling for the two cases in Sec. 3.1, where $R_{\text{TAR}} = 1.20$ m (black) and $R_{\text{TAR}} = 1.67$ m (red). (a) n_{TAR} , (b) T_{TAR} , and (c) Q_{\perp} are shown as a function of R with respect to the separatrix R_{SEP} . The experimental peak values are quoted in parenthesis adjacent to the SOLPS predictions.

Modeling of the radial sweep in R_{TAR} (Sec. 3.3) established that the baffle structure had an important role in determining divertor properties. For the endpoints of this sweep, i.e., $R_{\text{TAR}} = 1.21$ m and 1.30 m, SOLPS indicates that both T_{TAR} and Q_{\perp} would be reduced as R_{TAR} was swept from 1.21 m to 1.30 m. This result was largely in agreement with experiment, both qualitatively and quantitatively. In addition, n_{TAR} increased with R_{TAR} , in qualitative agreement with experiment but at only half the amount observed in experiment. Modeling shows that with greater proximity of the OSP to the baffle structure enhanced neutral trapping. Increased neutral trapping raised recycling activity, resulting in increased n_{TAR} and lowered T_{TAR} . This is consistent with observation. As R_{TAR} was drawn toward the baffle structure, neutral pressure measured in the lower divertor pumping plenum increased by a factor of 3–4, and D_{α} -activity increased by a factor of ≈ 2 . These observations suggest the increased presence of neutrals near the outer divertor target. Furthermore, the higher n_{TAR} and lower T_{TAR} conditions in the $R_{\text{TAR}} = 1.30$ m case resulted in an increase in radiated power along the outer divertor leg ($\approx 30\%$) and was clearly helpful in reducing Q_{\perp} .

Changing the parallel connection length in the SOL resulted in behaviors in n_{TAR} and T_{TAR} largely in agreement with the TPM, and inserting $L_{\parallel\text{-XPT}}$ for parallel connection length in Eqns (1) and (2) produced slightly better agreement with experiment than using $L_{\parallel\text{-MID}}$. The data showed that parallel connection length does play a role in determining in n_{TAR} and T_{TAR} . What is particularly interesting is that $[Q_{\perp}]^{\text{IR}}$ was *lower* in the case where f_{EXP} was also lower, i.e., the high X-point case, and that the FWHM of the heat flux profiles of both cases were equal. Increasing L_{\parallel} affected Q_{\perp} and its profile width as much as the geometric effects from increasing f_{EXP} . Modeling

suggests that increased cross-field transport effects were clearly in play, so that, as L_{\parallel} increased, the width of the heat flux at the target also increased.

In summary, we have found that the dependence of n_{TAR} and T_{TAR} on L_{\parallel} , as predicted by the TPM, was consistent with our data and that the importance of cross-field energy transport as parallel connection length was increased relative to poloidal flux expansion at the target was demonstrated. The dependence of n_{TAR} and T_{TAR} on R_{TAR} was in qualitative agreement with the TPM over the narrow range of R_{TAR} but not when plasmas with OSPs on the floor were compared with plasmas with OSPs on the baffle top. Preliminary SOLPS modeling suggests that this latter result may in part result from greater convected heat flux, driven by escaping neutrals, in the more open configuration when the OSP is on the *baffle top*.

REFERENCES

- [1] J.A. Goetz, *et al.*, J. Nucl. Mater. **266–269** (1999) 359.
- [2] J. Rapp, *et al.*, Nucl. Fusion **44** (2004) 312.
- [3] A. Kallenbach, *et al.*, J. Nucl. Mater. **337–339** (2005) 732.
- [4] T.W. Petrie, *et al.*, J. Nucl. Mater. **363–365** (2007) 416.
- [5] M. Kotschenreuther, Phys. Plasmas **14** (2007) 072502.
- [6] D. Ryutov, Phys. Plasmas **14** (2007) 06452.
- [7] P.C. Stangeby, (private communication).
- [8] R. Schneider, *et al.*, Contrib. Plasma Phys. **46** (2006) 3.
- [9] B.J. Braams, Contrib. Plasma Phys. **36** (1996) 276.
- [10] D. Reiter, *et al.*, Fusion Sci. Tech. **47** (2005) 172 and www.eirene.de.
- [11] J.M. Canik, *et al.*, J. Nucl. Mater. **415** (2011) S409.
- [12] P.C. Stangeby, *The Plasma Boundary of Magnetic Fusion Devices*, IOP Publishing (2002) Chapter 5.

ACKNOWLEDGMENT

This work was supported by the U.S. Department of Energy under DE-FC02-04ER54698, DE-AC05-00OR22725, DE-AC52-07NA27344, DE-AC04-94AL85000, DE-FG02-07ER54917, and DE-FG02-05ER54809.